The Life Cycles of Some Nonlinear Baroclinic Waves

ADRIAN J. SIMMONS AND BRIAN J. HOSKINS

U.K. Universities' Atmospheric Modelling Group, Department of Meteorology, University of Reading, England

(Manuscript received 30 August 1977, in final form 22 November 1977)

ABSTRACT

Some aspects of the nonlinear behavior of mid-latitude baroclinic waves are investigated by means of a series of integrations of the primitive equations with spherical geometry. Each integration has as initial conditions a balanced zonal flow perturbed by a small-amplitude disturbance of normal-mode form. Results are presented in detail for several zonal flows and perturbations which are confined initially to either zonal wavenumber 6 or zonal wavenumber 9.

In each case a disturbance grows by baroclinic instability and develops a structure in some agreement with the usual synoptic picture of an occluding system. Its growth rate at low levels decreases more rapidly than that at higher levels, as found by Gall using a more severely truncated model, and upper-level amplitudes become larger relative to surface values than in the initial linear mode. This is more marked for wavenumber 6 than for wavenumber 9, and differences in linear structure are thus enhanced in the nonlinear regime.

Barotropic processes become important during the occlusion of the disturbance as the forcing of vertical motion by thermal advection decreases in importance, although the vorticity actually changes at about half the rate that would occur in a barotropic fluid. In these examples the barotropic effects bring about a decay of the wave at a rate similar to that of its earlier baroclinic growth, and a well-defined life cycle exists.

Large-scale eddy fluxes of heat and momentum averaged over this life cycle have a structure that is substantially different from that given by linear stability analyses, and agreement with observation is improved. Net changes to the zonal-mean temperature gradient are largely confined to the lower troposphere and, to a lesser extent, the lower stratosphere. The change in surface zonal-mean flow is much as suggested by linear theory but at upper levels the westerly jet is strengthened as the disturbance decays.

Additional barotropic integrations have been performed to examine the changes in structure of longer wavelength disturbances at upper levels. Predominantly poleward momentum fluxes result from latitudinal variations in phase speed, and movement at a particular latitude is found to be governed largely by the zonal-mean velocity and vorticity gradient at that latitude. Additional baroclinic experiments provide an example of interactions involving a slower growing, longer wavelength component, and examples of some truncation errors that may result from use of lower resolution models. The sensitivity of results to the inclusion of dissipative processes is also examined.

1. Introduction

Following the original work of Charney (1947) and Eady (1949) there has been a widespread interest in the linear theory of baroclinic instability. However, while comparison with the observed development of large-scale mid-latitude disturbances has clearly identified the latter as commonly resulting from such an instability, there nevertheless remain a number of respects in which the results of linear theory differ significantly from observed statistics of the general circulation. Thus, despite recent extensions to the primitive equations with spherical geometry and high vertical resolution (Gall, 1976a; Simmons and Hoskins, 1976), linear solutions generally exhibit relatively large amplitude near the surface and may fail to represent the correct patterns and relative strengths of upper-level eddy fluxes (Green, 1970; Gall, 1976a; Simmons and Hoskins, 1977a). Such discrepancies, in addition to being of intrinsic interest, may be of significance for climate modeling since results of linear theory are an important part of several parameterizations of eddy fluxes used in zonally symmetric and low-resolution three-dimensional models (Schneider and Dickinson, 1974; White, 1977).

In this paper we investigate some aspects of the nonlinear behavior of mid-latitude baroclinic waves by means of a series of numerical integrations of the primitive equations with spherical geometry. Initial conditions comprise in each case a zonal, baroclinically unstable jet perturbed by a small-amplitude disturbance of predetermined normal-mode form. This work is thus a natural extension of that by Simons (1972) using a quasi-geostrophic model and Gall (1976b) using the primitive equations, both of whom followed the growth of baroclinic waves into the nonlinear regime using a numerical truncation more severe than that

0022-4928/78/0414-0432$09.50

adopted here. The present integrations provide a more complete representation of the occlusion of the wave and confirm several findings of the earlier studies, although there are differences in detail.

A novel feature of our results is that the occlusion is followed by a pronounced decay of wave amplitude during which barotropic processes dominate. The disturbances thus possess a well-defined life cycle, and net eddy fluxes and zonal-mean changes calculated over the whole life cycle may be compared with patterns given by linear theory. Attention is concentrated here on such aspects of the solutions. A more detailed study of the synoptic development, with particular emphasis on frontogenesis, will be given elsewhere.

It should be noted that use of normal-mode initial conditions implies a sequence of identical disturbances —both upstream and downstream. In addition, the motion is described here by equations which are inviscid and adiabatic apart from an internal dissipation required to limit frontal formation to a resolvable scale, and we include no forcing at the lower boundary. Thus, in comparison with the real atmosphere, we consider a much idealized situation. This has the advantage of enabling results to be more easily related to previous simpler studies, but yields a rather specific type of mature behavior. A gradual relaxation of some of the simplifying assumptions will be made in subsequent studies.

2. The numerical model

The basic numerical model used for this study is that described in detail by Hoskins and Simmons (1975). The primitive equations are expressed in sigma coordinates and in vorticity and divergence form. Variables are represented in the horizontal by truncated expansions in terms of spherical harmonics and in the vertical by their values at discrete levels. A second order semi-implicit time scheme is used, and here we incorporate the filter suggested by Robert (1966), as in our linear studies of baroclinic instability (Simmons and Hoskins, 1976).

For most of the present experiments the horizontal resolution comprises a triangular spectral truncation at total wavenumber 42, which gives a shortest retained scale of 150 km, although interactions involving this scale are poorly represented. In the vertical 14 unequally spaced levels are used, these being chosen to give a resolution everywhere less than 100 mb, with enhanced resolution close to the ground and a limited resolution of the lower stratosphere. The actual level spacing is specified later in Table 2. A timestep of $\frac{1}{2}$ h is used. A few experiments have been performed using different resolutions, and these are discussed in Section 10.

Our particular interest here is in the dynamical aspects of the life cycle of the disturbances, and integrations have thus been performed incorporating few additional physical processes. In fact, for most cases the only such process included is an internal diffusion in which terms $-\kappa\nabla^2(\nabla^2\xi)$, $-\kappa\nabla^2(\nabla^2 D)$ and $-\kappa\nabla^2(\nabla^2 T)$ are added to the expressions for the rates of change of relative vorticity ξ, divergence D and temperature T. Here ∇^2 is the two-dimensional Laplacian operator and $\kappa = 2.338\times10^{16}$ m^4 s^{-1}. Some such form of internal smoothing is needed in experiments such as these in order to prevent the attempted formation of fronts on scales that cannot be resolved, and it is hoped that the energy thus dissipated is typical of that which would be transferred to such scales in reality. The present choice is simple to include in a spectral model, and is suitably scale selective, giving a decay rate of $(\frac{1}{4}$ day$)^{-1}$ for the shortest retained scale but having little effect on the larger scales associated with the growing baroclinic wave. The value of κ was chosen somewhat subjectively as the smallest that maintained coherent fields of vorticity and divergence. Integrations using different values give similar results, and these are also discussed in Section 10, together with results from several integrations including other physical processes.

3. Initial conditions

Each integration has as initial conditions a zonal jet perturbed by a small-amplitude disturbance of normal-mode form. For a given zonal wavenumber this mode is predetermined by applying an initial-value technique to a linearized, adiabatic version of the numerical model. Full details of the method of calculation have been given by Simmons and Hoskins (1976). When used as initial conditions for a nonlinear integration each mode is scaled to give an initial surface pressure wave of amplitude 1 mb.

The zonal flows chosen for study here are those whose linear stability was examined by Simmons and Hoskins (1977a) and reference should be made to the latter paper for a detailed description of both the zonal-mean states and the structure and transfer properties of the most unstable normal-mode disturbances. The four flows examined each have a maximum at 200 mb, and will be referred to by their horizontal structures, which comprise jets of relatively broad meridional scale centered at 30° and 55° latitude, a jet centered at 45°, and a second 30° jet of smaller meridional scale. These flows are not intended to model in detail any specific observed or climatological profile, and should be regarded as particular examples from a range of possible atmospheric flows. A feature of our results is that the qualitative nature of solutions varies little from flow to flow, and for purposes of presentation we concentrate on results for the 45° jet.

For each particular zonal flow it is necessary to choose the zonal wavenumber of the initial normal-mode disturbance. Integrations have been performed using wavenumber 6 perturbations for all flows, and using wavenumber 9 perturbations for all but the 55° jet,

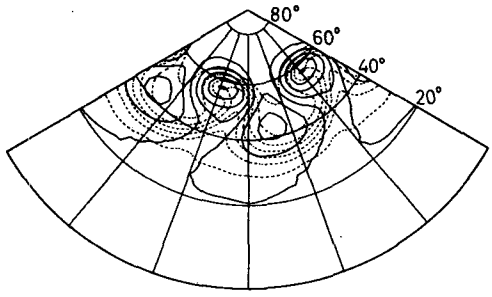

FIG. 1. North polar stereographic plot showing surface pressure (solid contours) and low-level temperature ($\sigma=0.985$, broken contours) after seven days of integration for the wavenumber 6 perturbation to the 45° jet. Contours are drawn at intervals of 8 mb and 4°C using linear interpolation between values on the computational grid comprising 32 "Gaussian" latitudes and 32 regularly spaced points per 60° longitude. Background lines of latitude and longitude are drawn at intervals of 20°.

for which the higher wavenumber modes appear to be atypical (Simmons and Hoskins, 1977a). These two wavenumbers are among the faster growing for these flows. Additional integrations using wavenumber 3 and wavenumber 12 initial conditions have been performed for the broader 30° jet.

4. Some synoptic features

In this section we illustrate a limited number of synoptic features for the case of wavenumber 6 initial conditions and the 45° jet. A more complete description of fields related to the frontal formation and occlusion of the disturbance will be given elsewhere. Here we present a single picture of the low-level structure of the occluding wave, and show the upper-level flow pattern during the period of final growth and subsequent barotropic decay. The net effect of the disturbance on the temperature disturibution at several levels is also shown.

The surface pressure and low-level temperature after seven days of integration are illustrated in Fig. 1. By this time the surface low has deepened to an amplitude of about 32 mb and moved some 8° poleward to a position 12° north of the jet maximum. There is a larger area of weaker high pressure to the south. The temperature wave shows a pronounced distortion, with the strongest gradients located in positions typical of occluded and cold fronts, and the region of relatively warm air has diminished as the wave develops. These and other fields are in close agreement with the usual synoptic picture of an occluding mid-latitude distance. Little further intensification occurs at the surface beyond this time.

The streamfunction at an upper tropospheric level is illustrated in Fig. 2 for day 8[1] and the five following days. The sequence shows the disturbance continuing to grow up to a time between day 9 and day 10, during which there is a gradual enhancement of the southwest to northeast tilt to the south of the disturbance maximum and a reduction of the opposite tilt to the north. In the absence of vertical coupling such a pattern would imply a barotropic strengthening of the jet and decrease in wave amplitude. Just such a process is observed to occur rapidly beyond day 10. During this time the

[1] Eight days after the start of the integration.

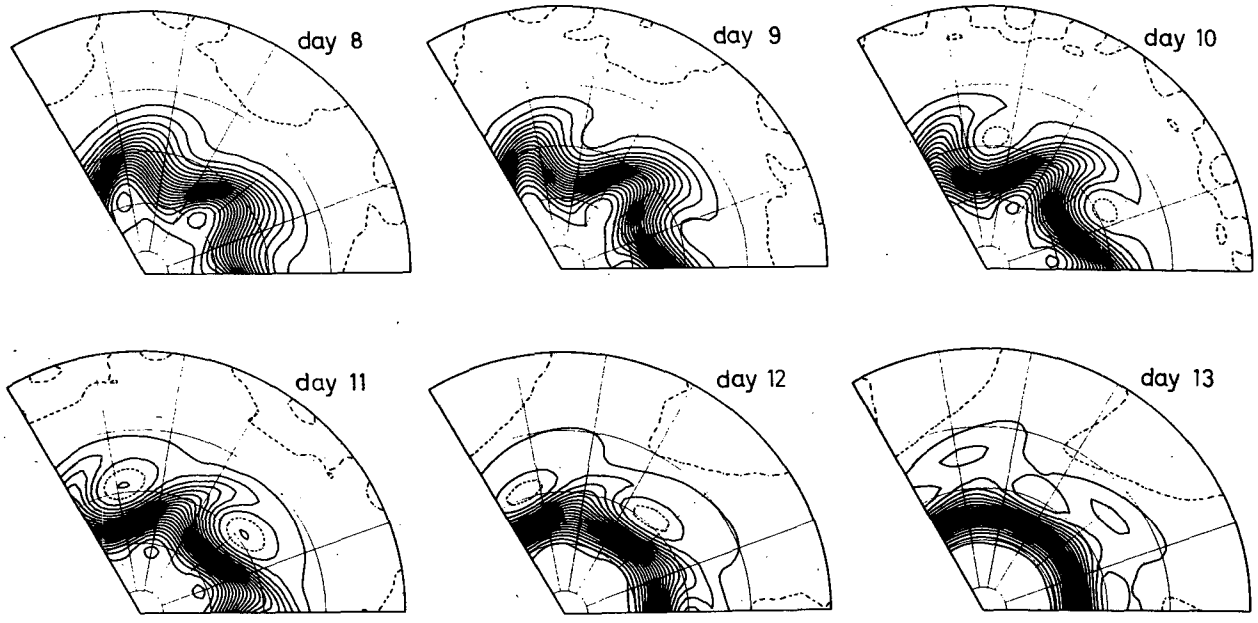

FIG. 2. Streamfunction at $\sigma=0.321$ at daily intervals from day 8 to day 13 for the wavenumber 6 perturbation to the 45° jet. The zero contour is dashed to avoid emphasis of insignificant small-amplitude variability close to the equator, and the contour interval is $1.5\times10^{-3}\ a^2\Omega$, where a is the radius of earth and Ω its angular velocity.

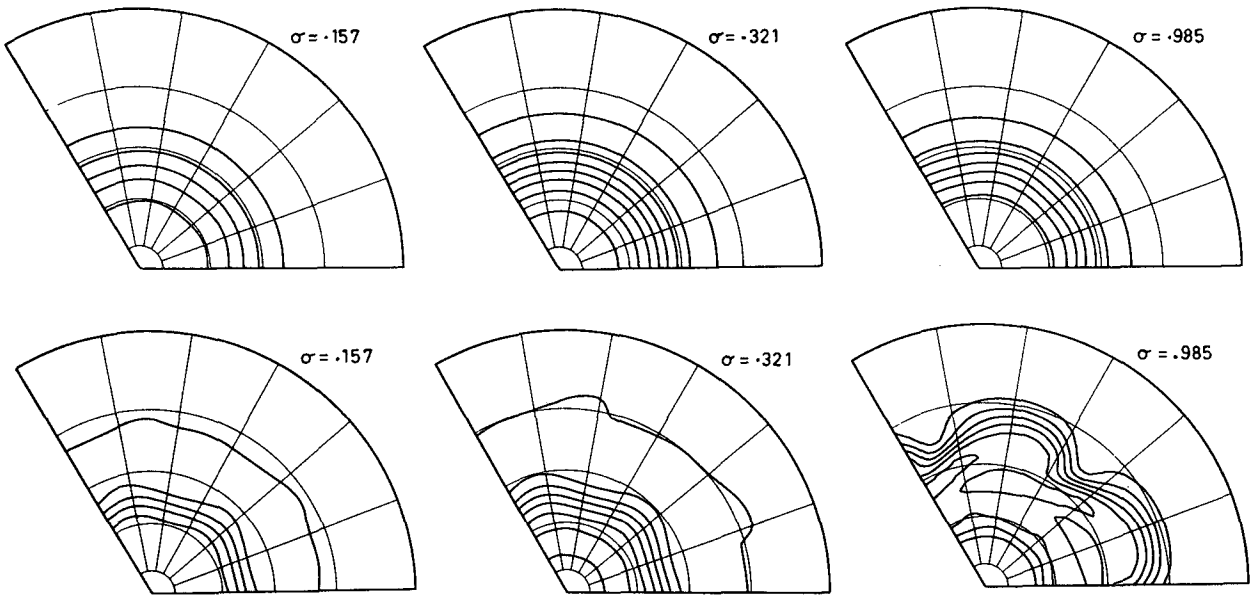

FIG. 3. Temperature at $\sigma=0.157$, 0.321 and 0.985 at days 0 (upper) and 14 (lower) for the wavenumber 6 perturbation to the 45° jet. The contour interval is 4°C.

tilt of the wave is from southwest to northeast at almost all latitudes and the corresponding eddy momentum flux is almost entirely poleward.

A similar sequence occurs at other upper tropospheric and lower stratospheric levels. Such pronounced tilts are not evident in patterns of low-level streamfunction, but here too there is a significant loss of eddy energy between days 10 and 12 and an enhancement of the easterly-westerly-easterly distribution of surface zonal-mean wind forced by the wave in its growing phase.

The initial temperature field and that after 14 days are shown in Fig. 3 for the model level closest to the surface and for levels in the upper troposphere and lower stratosphere. Near the surface the net effect of the disturbance is to destroy the marked temperature gradient between latitudes 40° and 60°, but to enhance gradients to the south and north. Static stability is also enhanced in these regions, and although a remnant of the original wave can be seen at day 14 in the southern zone, we find no significant secondary development in integrations continued to day 27.

Quite different temperature changes are found at higher levels. In the upper troposphere, although there is some weakening of the overall baroclinic zone there is little change in the gradient between latitudes 40° and 60°. In the lower stratosphere the baroclinic zone is weakened to the south, but the reversed gradient is enhanced between 45° and 60°.

Results for wavenumber 9 initial conditions are generally similar to those for wavenumber 6 at low levels, although variations in amplitude are apparent. The principal difference is that the shorter wavelength disturbance remains concentrated at low levels throughout the course of the integration. At upper levels a relatively weak perturbation grows and decays retaining much of the structure of the normal mode, being concentrated poleward of the jet maximum with a tilt such as to give a predominantly equatorward momentum transfer, as will be illustrated subsequently.

5. Energetics

The energetics of each integration have been evaluated at daily intervals using the expressions derived by Lorenz (1955) for pressure coordinates. To apply these, fields were linearly interpolated from sigma coordinates at each point of the grid used for the computation of nonlinear terms, and for simplicity derivatives were evaluated using finite differences. In spite of the errors introduced by both this procedure and the approximate nature of the energy equations an error of less than 10% was found in a check of the components of the energy balance over the life cycle of the wavenumber 6 disturbance to the 45° jet.

The variation with time of the eddy energy is shown in Fig. 4 for zonal wavenumbers 6 and 9 and various flows. In all cases growth of a disturbance is followed by a period during which it decays at much the same rate as that at which it grew, and it is clear that well-defined life cycles exist. For clarity the result for the wavenumber 6 disturbance to the sharper 30° jet is not shown in Fig. 4 but it too exhibits the same overall behavior, with a slow growth to a relatively weak maximum eddy energy of 0.73×10^5 J m^{-2} at day 17, and a slow subsequent decay.

The results for different flows reveal substantial variations in the maximum eddy energies reached by disturbances of a given zonal wavenumber. Maximum

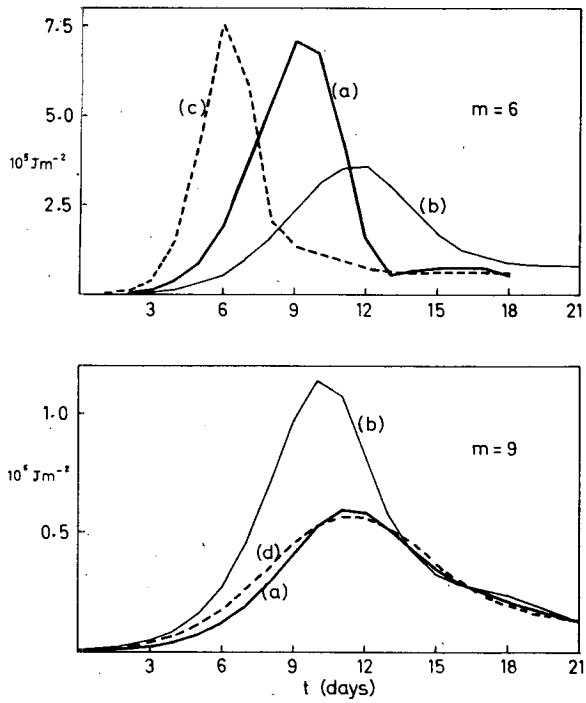

FIG. 4. Variation with time of the sum of eddy kinetic and eddy available potential energy for wavenumber 6 (upper) and wavenumber 9 (lower) disturbances to (a) the 45° jet, (b) the broad 30° jet, (c) the 55° jet and (d) the narrow 30° jet. The different scales of the upper and lower graphs should be noted.

values are found to be attained within about three days from the time the meridional temperature gradient first reverses at the surface, and determination of the most unstable normal mode for the zonal-mean state at this time indicates that a marked change of structure would be required to achieve further (but much weaker) baroclinic growth. What appears to happen here is that barotropic processes bring about a decay of amplitude, and further zonal-mean changes, before such an adjustment can be completed. As growth ceases there remains a considerable amount of zonal available potential energy, the largest depletion amounting to little more than a quarter of that initially present. Thus the indication from these results, and those of Gall (1976b), is that growth is limited largely by a local stabilization of the flow, rather than by the overall amount of available energy as argued by Green (1970).

For a particular wavenumber Fig. 4 shows a tendency for larger maximum eddy energies to be associated with larger growth rates in the linear phase. Given that growth is indeed limited by the first reversal of the meridional temperature gradient, this result is as suggested by linear theory for a mode growing as $\exp(gt)$ inducing zonal-mean changes at a rate $\exp(2gt)$, but beyond such considerations it is difficult to evaluate in a precise quantitative way the factors determining maximum values. Assuming exponential growth to be maintained for finite-amplitude disturbances, linear solutions give times for the reversal which are typically two days earlier than computed for wavenumber 6, but variations in nonlinear growth are such that amplitudes at the predicted time of reversal are poor indicators of those actually reached, giving eddy kinetic energies too small by a factor which varies from 2.5 for the broad 30° jet to 9.5 for the 45° jet.

In addition to variations from flow to flow, the energy levels reached by wavenumber 6 disturbances are generally substantially larger than those reached by wavenumber 9, in agreement with a result found by Gall (1976b). In these examples this is associated principally with the very much larger upper-level amplitudes of the wavenumber 6 disturbances. For the 45° jet the surface eddy kinetic energy density is also larger for wavenumber 6 than for wavenumber 9, but the reverse is true for the two 30° jets, for which wavenumber 9 has the faster linear growth rate. Wavenumber 6 is the faster growing for the 45° jet.

An example of the variation with time of the various energy conversions is given in Fig. 5 for the wavenumber 6 disturbance to the 45° jet. Up to day 8 baroclinic processes evidently dominate, with conversions from zonal to eddy available potential energy and from the latter to eddy kinetic energy. As these conversions decrease in magnitude the barotropic conversion from eddy to zonal kinetic energy becomes dominant, as found by Simons (1972), here reaching a maximum value at day 11 when the baroclinic conversions have decreased almost to zero. Although at each day the

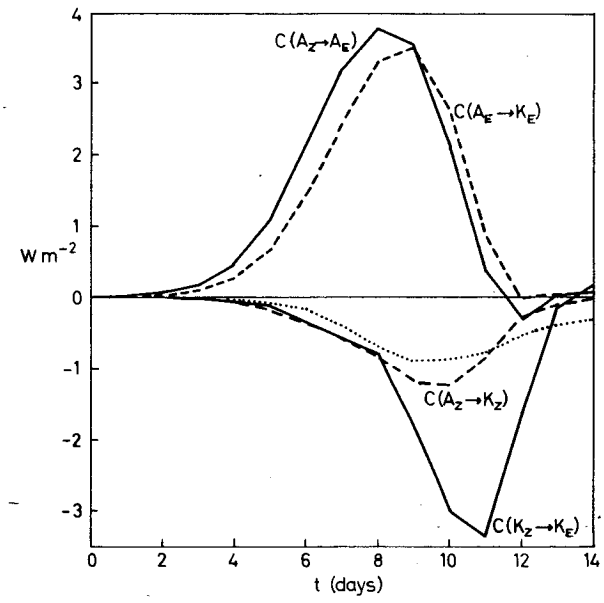

FIG. 5. Variation with time of various energy conversions and the net rate of energy dissipation (dotted curve) for the wavenumber 6 disturbance to the 45° jet. A_Z and A_E are the zonal and eddy available potential energies, and K_Z and K_E the corresponding kinetic energies. Positive values of $C(A_Z \rightarrow A_E)$ imply a transfer from A_Z to A_E, and negative values imply a reversed transfer.

internal dissipation is weak compared with the major conversions, its overall effect is significant, the net loss of zonal available potential energy being slightly more than twice the gain of zonal kinetic energy.

A similar cycle is found in other cases. Internal dissipation becomes relatively larger in the energy budget of the wavenumber 9 disturbances, but little overall change is found in results from an experiment in which the diffusion coefficient was halved. Further discussion is given in Section 10.

A feature of the nonlinear growth of many disturbances is the development of amplitudes that are substantially larger at upper levels than close to the surface. This is illustrated for the wavenumber 6 disturbance to the 45° jet in Fig. 6, which shows the distribution with latitude and height of the eddy kinetic energy density at days 0 and 10, and the distribution averaged over the 10 day period from day 4 to day 14. At day 10 the eddy kinetic energy is a maximum, and the contribution from about this time dominates the average over the life cycle, as is the case for many other fields.

The relative enhancement of upper level amplitudes is generally greater in these examples than in that considered by Gall (1976b) who, while finding some upper level increase in the horizontally averaged kinetic energy density, showed the surface maximum in geopotential perturbation to remain slightly larger than the upper tropospheric maximum throughout the integration. However, the extent of the enhancement is found here to vary significantly from flow to flow, being (for kinetic energy) about four times larger for the narrower 30° jet than for the 55° jet, which shows little upper level increase. The enhancement is also larger by a factor of about 2 for wavenumber 6 than for wavenumber 9, the nonlinear regime thus amplifying differences in upper level amplitude found in normal-mode studies.

Further investigation has been made for the wavenumber 6 disturbance to the 45° jet. It is found that vertical energy transfer plays a relatively small role in the separate kinetic energy budgets of the upper and lower troposphere. Larger upper level amplitudes may thus be viewed as resulting from a larger upper level conversion of eddy available potential energy to eddy kinetic energy, as found by Gall. This in turn may be linked with the tendency inherent in normal-mode results for zonal-mean changes to be concentrated at the surface, thus leaving an upper level structure initially more suitable for further baroclinic growth than that at lower levels. This lasts only for a limited period of time, and upper-level growth ceases as barotropic effects become dominant.

6. Eddy fluxes and the mean meridional circulation

In this section we discuss the eddy fluxes of heat and momentum, and the induced mean meridional

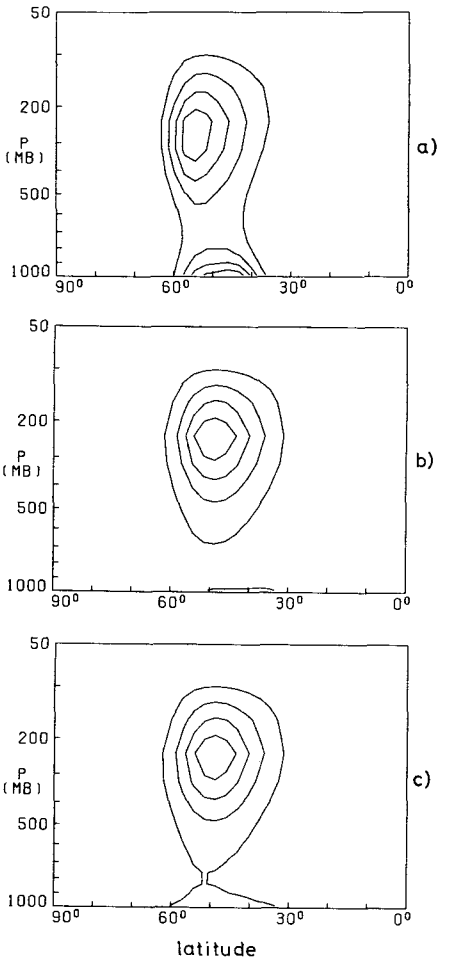

FIG. 6. Meridional cross sections of eddy kinetic energy density $[\frac{1}{2}(\overline{u'^2+v'^2})]$ at (a) day 0, (b) day 10, and (c) averaged from day 4 to day 14, for the wavenumber 6 disturbance to the 45° jet. Here u' is the zonal velocity perturbation, v' the meridional velocity perturbation, and the overbar denotes a zonal average. For this and subsequent sections values are linearly interpolated to pressure coordinates using a mean surface pressure of 1000 mb. Contours are drawn using linear interpolation between values defined on the computational grid, and the interval is one-fifth the maximum value of each field. Dimensional values of various averaged fields are given in Table 1. The maximum density of K_E at day 10 is about 530 m^2 s^{-2}.

circulation, concentrating on values averaged over the life cycles of the disturbances. To enable specific comparisons to be made between the results for different wavenumbers and different flows, an averaging period of 10 days has been chosen in each case. The actual times are specified subsequently in Table 1.

Meridional cross sections of averaged poleward eddy heat fluxes for the wavenumber 6 integrations are presented in Fig. 7. In comparison with linear calculations (Simmons and Hoskins, 1977a) upper tropospheric fluxes are of significantly larger relative amplitude, and results now exhibit the observed secondary upper tropospheric maximum (Oort and Rasmusson, 1971;

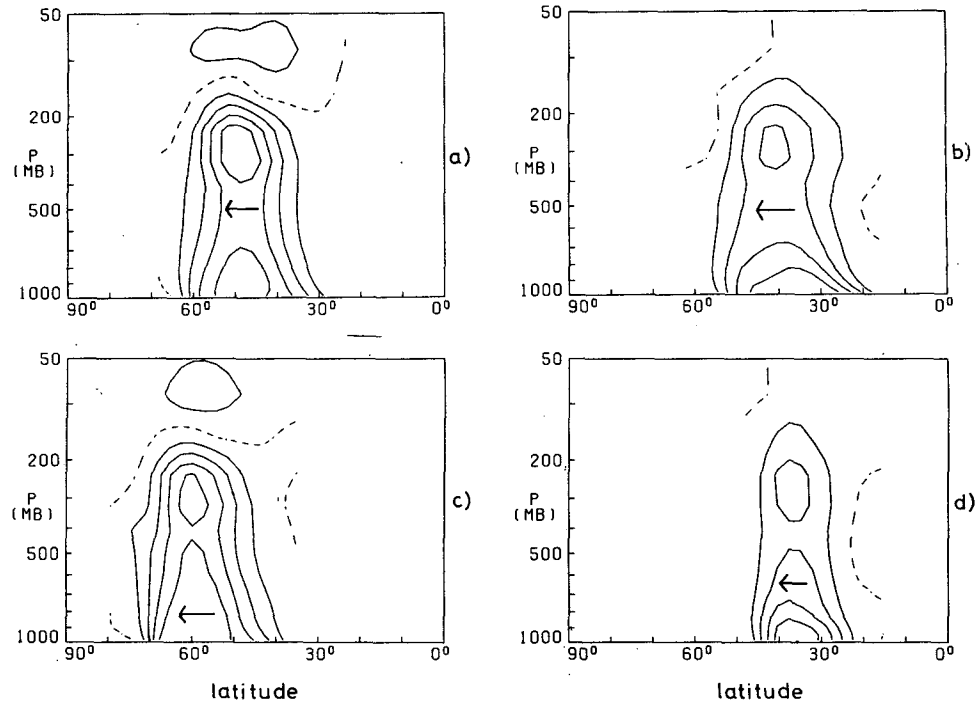

FIG. 7. Meridional cross sections of time-averaged horizontal eddy heat fluxes $\overline{v'T'}$ for wavenumber 6 disturbances to (a) the 45° jet, (b) the broad 30° jet, (c) the 55° jet and (d) the narrow 30° jet. Here T' is the temperature perturbation and the direction of each flux is indicated by an arrow. The zero contour is dashed and drawn only at those latitudes where the amplitude at some level exceeds one-tenth of the contour interval.

Newell *et al.*, 1974). Fluxes are also of broader meridional scale, particularly at low levels where the location of the maximum varies over a range of up to 20° of latitude as the zonal-mean temperature gradient weakens and reverses in middle latitudes. Significance should not be attached to the reversed flux above 150

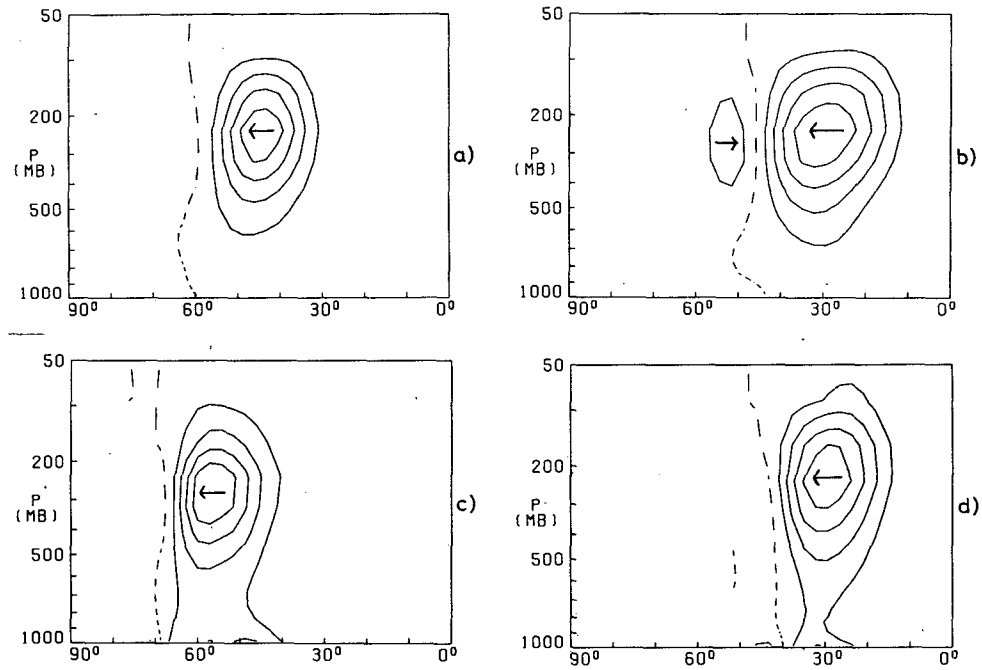

FIG. 8. Meridional cross sections of horizontal eddy momentum fluxes $\overline{u'v'}$ for the same cases as in Fig. 7.

mb for the 45° and 55° jets since repetition of the calculation for the 45° jet using an improved stratospheric resolution resulted in a halving of its magnitude. In addition, the basic zonal-mean flows are unrepresentative of either the summer or the winter stratosphere at the uppermost layers.

The corresponding patterns of poleward eddy momentum fluxes are illustrated in Fig. 8, and exhibit much less variation from flow to flow than is the case for the linear modes. Increases in upper level amplitude and changes in tilt as the waves mature and decay are reflected in momentum fluxes which in all cases are concentrated in the upper troposphere, with predominant poleward maxima located at latitudes close to those of the initial jet maxima. Such results are in good agreement with observed net transient eddy fluxes (Oort and Rasmusson, 1971; Newell *et al.*, 1972). Analyses by Blackmon *et al.* (1977) show significant equatorward components for disturbances with 2.5–6 day periods, but the wavenumber 6 disturbances examined here have periods close to the low-frequency end of this range and, as discussed below, wavenumber 9 disturbances are associated with predominantly equatorward components, although these are of small amplitude.

Averaged horizontal eddy heat and momentum fluxes for the wavenumber 9 disturbance to the 45° jet are shown in Fig. 9. Results for the other zonal flows are again remarkably similar. For this wavenumber, averaged fluxes are closer in form to those given by linear calculations, and although there is some increase in vertical scale the poleward heat flux remains largely confined to the lower troposphere. As noted above the eddy momentum flux has a much stronger equatorward than poleward component, in marked contrast with the results for wavenumber 6, differences in linear structure again being amplified in the nonlinear regime.

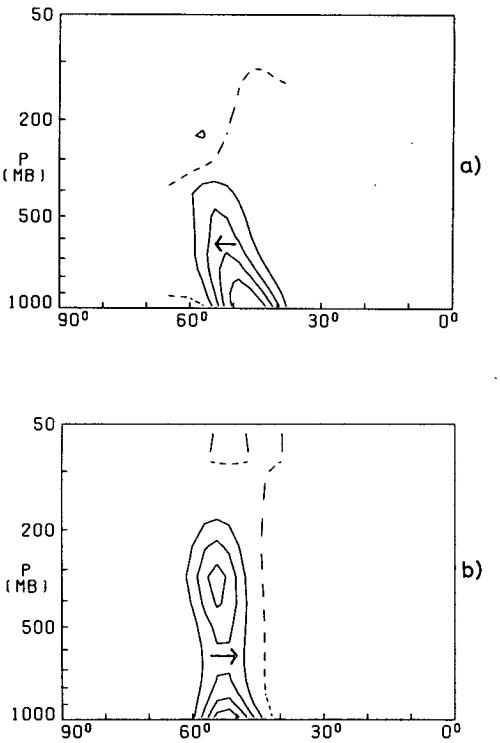

FIG. 9. Meridional cross sections of (a) the time-averaged horizontal eddy heat flux and (b) the corresponding momentum flux for the wavenumber 9 disturbance to the 45° jet.

An indication of the magnitudes of the averaged horizontal eddy fluxes is given in Table 1. As with the net eddy energies there are considerable overall variations from flow to flow, but concentrating attention on the *relative* magnitudes of upper-level heat and momentum fluxes for wavenumber 6 initial conditions, we find a significant difference from the corresponding results for linear modes (Table 1, Simmons and Hoskins, 1977a). As suggested by the synoptic pictures and

TABLE 1. Amplitudes of the upper and lower level maxima in poleward eddy heat flux ($\overline{v'T'}$), the upper level maximum in horizontal eddy momentum flux ($\overline{u'v'}$), and the maximum eddy kinetic energy density [$\frac{1}{2}(\overline{u'}+\overline{v'})$], for 10-day averages. Positive values for the momentum flux denote a maximum poleward flux and negative values a maximum equatorward flux. Kinetic energy densities are largest near the tropopause for wavenumber 6 and at the surface for wavenumber 9.

Zonal flow	Averaging period (days)	$\overline{v'T'}$ (lower) (°C m s^{-1})	$\overline{v'T'}$ (upper) (°C m s^{-1})	$\overline{u'v'}$ (m^2 s^{-2})	$\frac{1}{2}(\overline{u'^2}+\overline{v'^2})$ (m^2 s^{-2})
Zonal wavenumber 6					
45° jet	4–14	19.2	20.1	106.4	219
55° jet	1–11	22.1	20.1	80.2	146
30° jet broad	6–16	11.9	7.9	47.0	67
30° jet narrow	10–20	5.5	2.7	15.7	28
Zonal wavenumber 9					
45° jet	6–16	5.0	—	−12.6	44
30° jet broad	5–15	7.3	—	−13.2	46
30° jet narrow	6–16	5.7	—	−5.3	27

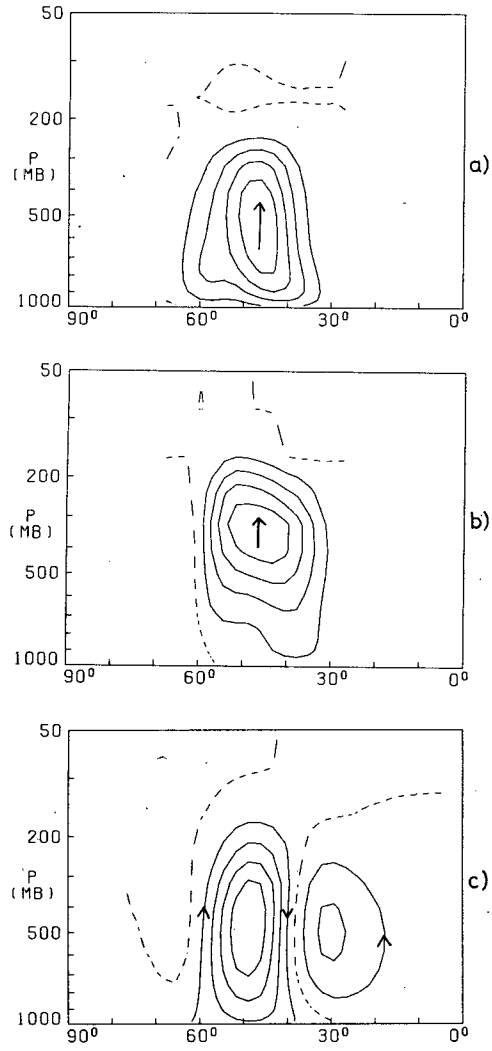

FIG. 10. Meridional cross sections of time-averaged values of (a) the vertical eddy heat flux $\overline{\omega' T'}$, (b) the vertical eddy momentum flux $\overline{\omega' u'}$ and (c) the streamfunction of the mean meridional circulation for the wavenumber 6 disturbance to the 45° jet. Here ω is the usual material derivative of pressure, and maximum dimensional values are 7.8°C mb h^{-1}, 12.3 m s^{-1} mb h^{-1} and 108 m s^{-1} mb, respectively.

energetics discussed earlier, there is a gradual increase in the strength of the upper poleward momentum flux relative to the heat flux throughout the growth of each disturbance, and in the decay stage the heat flux decreases to a negligible value one or more days before the momentum flux. The overall effect is that the relative strength of the averaged momentum flux is between two and three times larger than found for the normal mode. Comparison with observed transient eddy fluxes compiled by Oort and Rasmusson (1971) shows that, if maximum upper level heat fluxes are scaled to agree, our computed momentum fluxes are generally weaker than observed winter values but stronger than observed in other seasons.

In general, specific comparisons with atmospheric circulation statistics are not straightforward. The statistics themselves show quite large variations from month to month, and with transient eddy disturbances occurring in the atmosphere on a range of scales it is not clear what combination of wavenumbers 6 and 9 is appropriate, or indeed whether 6 and 9 are sufficiently representative of other wavenumbers likely to be present with significant amplitude. However, following the approach adopted in the preceding paragraph, if it is assumed that the structure of wavenumber 6 is representative at upper levels it is evident that the eddy kinetic energy is weaker relative to eddy fluxes than is the case for observed transient eddy statistics. This may well be in part due to the specific nature of the present experiments in which much of the disturbance energy is quickly transferred to the mean state rather than, for example, to a lower wavenumber, as indicated subsequently in the context of an experiment with wavenumber 3 initial conditions. In addition, a discrepancy may also arise because of a significant contribution to the eddy velocity statistics from transients other than unstable baroclinic waves, as has been argued by Green (1970).

It should also be noted that although for wavenumber 6 the structure and ratio of poleward momentum and heat fluxes appear to be in reasonable agreement with observation, the net conversion from eddy to zonal kinetic energy is about two-thirds that from zonal to eddy available potential energy, and thus is relatvely larger than is generally the case in estimates based on atmospheric observations (e.g., Newell *et al.*, 1974). This is not necessarily inconsistent as the main contribution to the barotropic conversion is obtained from the product of two terms, one of which (the poleward eddy momentum flux) is a maximum close to a zero of the other (the meridional gradient of the zonal-mean zonal velocity), and results may thus be sensitive to small differences in the position of the flux maximum relative to the jet maximum. The discrepancy nevertheless raises again a question as to the generality of our results, a subject returned to briefly in our concluding paragraph.

An example of the patterns of averaged vertical eddy heat and momentum fluxes and the mean meridional circulation is given for wavenumber 6 in Fig. 10. A feature of linear baroclinic instability theory is a good correlation between poleward and upward motion, and here such a correlation remains over the whole life cycle. Thus directions and magnitudes of vertical fluxes follow closely those of the horizontal fluxes. The upward heat flux has a broad mid-tropospheric maximum indicating significant contributions to zonal-mean changes only near the ground and in the upper troposphere. In these regions magnitudes reach values in excess of half the maximum value of the convergence of the horizontal flux. The vertical flux of westerly

momentum is also predominantly upward, with an upper tropospheric maximum. Its convergence near the tropopause amounts to at most about one-fifth of the maximum convergence of the horizontal flux.

The mean meridional circulation differs from that induced by the normal mode in that there is an increase in the relative strength of the cell equatorward of the jet maximum, and a reduction in the polar cell. In the quasi-geostrophic approximation the mean circulation is determined by eddy heat and momentum fluxes and acts to maintain thermal-wind balance. The change noted here is consistent with the enhanced upper-level poleward momentum flux discussed previously.

7. Zonal-mean changes

The eddy fluxes of heat and momentum are of interest from the viewpoint of the comparison with general circulation statistics, and for their implications for the parameterizations required by zonally symmetric climate models. However, because of the important role of the mean meridional circulation they do not by themselves allow a direct deduction of net changes to the zonal-mean state. Some indications of these changes have been given in conjunction with the synoptic illustrations given in Section 4, and here we consider some further detail, principally for wavenumber 6 initial conditions.

The different regimes of baroclinic growth and barotropic decay are clearly illustrated in Fig. 11, which shows the strength of the maximum upper level zonal-mean flow as a function of time for the 45° jet. A feature of normal-mode solutions is a relatively small induced upper level change to the zonally averaged state, and this result appears from Fig. 11 to continue to hold up to about the time of maximum disturbance energy, day 9, although by this time some change in shape of the upper level jet has occurred, the maximum being located some 5° nearer the pole.

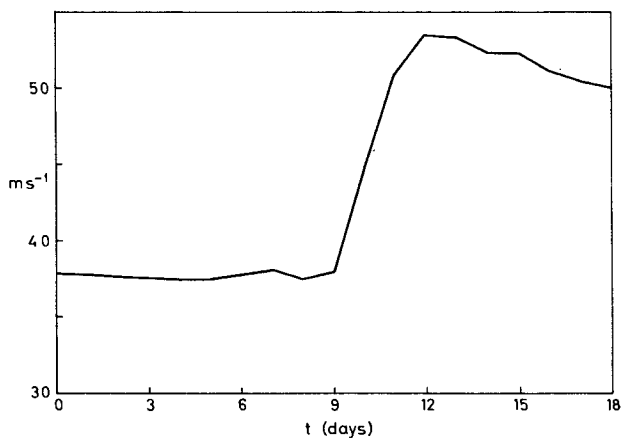

FIG. 11. Variation with time of the maximum zonal-mean velocity in the case of the wavenumber 6 disturbance to the 45° jet.

TABLE 2. The difference in zonal-mean temperature between latitudes 43.3° and 54.4° at days 0, 9 and 14, and the change from day 0 to day 14, for the case of the wavenumber 6 disturbance to the 45° jet. Values are plotted at pressure levels corresponding to the σ-levels used in the model. The actual σ-levels are obtained by division by 1000 mb. The figures in parentheses in the final column show, for comparison, the change from day 0 to day 15 in an experiment with surface friction. This is discussed in Section 10.

p (mb)	Temperature difference (°C) Day 0	Day 9	Day 14	Change (Day 14−Day 0)
27	0	−1.9	−2.3	−2.3 (−0.2)
87	−13.8	−11.5	−15.8	−2.0 (−2.6)
157	−8.0	−7.9	−11.6	−3.6 (−2.6)
236	6.2	3.8	3.6	−2.6 (−1.1)
321	12.6	9.1	11.8	−0.8 (1.0)
410	12.9	8.9	12.4	−0.5 (1.4)
500	12.7	8.0	11.5	−1.2 (1.2)
590	12.5	6.7	9.8	−2.7 (0.7)
676	12.4	5.3	7.9	−4.5 (0.0)
757	12.3	3.8	6.0	−6.3 (−0.8)
831	12.0	2.0	3.7	−8.3 (−2.2)
895	12.0	0.2	1.5	−10.5 (−4.7)
947	12.0	−1.3	−0.5	−12.5 (−8.1)
985	11.9	−2.2	−1.5	−13.4 (−11.4)

Rapid production of a stronger jet of smaller meridional extent takes place over the next three days as the wave decays, and this is followed by a slow decrease in the strength of the jet. During the latter there is a weak transfer of zonal to eddy kinetic energy, and the internal dissipation of zonal kinetic energy is of the same order. A stability analysis at day 14 shows the sharper jet formed during the decay of the disturbance to be barotropically unstable, but no significant subsequent growth of eddy energy occurs.

Qualitatively similar results are found at upper levels for other flows, the extent of the strengthening of the jet being dependent on the amplitude reached by the growing disturbance. As mentioned in Section 4 there is a general tendency for an easterly-westerly-easterly distribution of surface zonal-mean flow to be maintained throughout the life cycle, although its meridional scale increases from that illustrated by Simmons and Hoskins (1977a) for the linear mode. It is not surprising that the magnitude of the surface change is one of the few aspects of our results particularly sensitive to the inclusion of surface friction, as is discussed later.

Overall temperature changes for the 45° jet have been illustrated at three model levels in Fig. 3. Further detail is given in Table 2 which shows the temperature differences across 11° of latitude at the center of the initial baroclinic zone for each model level and days 0, 9 and 14. Considering first tropospheric levels we note a general reduction in the temperature gradient over the growth stage of the disturbance, the reduction being largest at the surface, as indicated by linear theory. Subsequently, the gradient is replaced in the

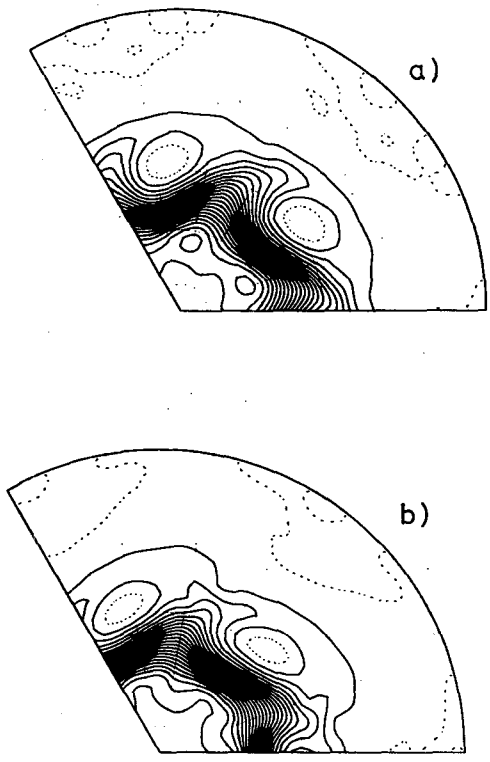

FIG. 12. Streamfunction after (a) 12 h and (b) 1 day from an integration of the barotropic vorticity equation which used as initial conditions the field at day 10 shown in Fig. 2.

decay stage by an amount which is insignificant near the surface, but sufficient above 500 mb to almost completely cancel the reduction that occurred during growth. The latter change occurs as the upper level jet strengthens, and is consistent with the maintenance of thermal-wind balance by the mean meridional circulation. The latter is determined at this time principally by the eddy momentum flux.

Because of limited stratospheric resolution quantitative significance should not be attached to the temperature changes at the uppermost levels. Here most change occurs during the decay stage with the reversed temperature gradient being enhanced above the strengthened westerly jet, again in keeping with thermal-wind balance. A similar result is found in an integration with higher stratospheric resolution, but the increase in gradient is about 50% larger close to 150 mb and smaller above about 100 mb. As illustrated in Fig. 3 the temperature gradient is weakened nearer the equator, this being associated with a weakening of the zonal-mean flow in this region as the jet is strengthened nearer the pole.

As has already been noted upper level amplitudes of the wavenumber 9 disturbances are substantially smaller than those of wavenumber 6, and give rise to insignificant zonal-mean changes at such levels. Surface changes are qualitatively similar to those found for wavenumber 6.

8. Some barotropic integrations

The energy conversions shown in Fig. 5 and the sequence presented in Fig. 2 illustrating the upper level decay of wave amplitude suggest the dominance of barotropic processes following the occlusion of the disturbance. To investigate this further a series of integrations of the barotropic vorticity equation has been performed. In these we examine the subsequent behavior of a large-amplitude disturbance superimposed on a zonal flow. Examples of such an approach are to be found in the work of Platzman (1952) and Kuo (1953). In the following section we present a quasi-geostrophic analysis which clarifies the relationship between these barotropic results and those obtained using the primitive equations.

The first set of barotropic integrations used as initial conditions vorticity fields at an upper tropospheric level ($\sigma=0.321$) from the full primitive equation model at times close to those of maximum eddy energy. For the wavenumber 6 disturbance to the 45° jet the actual time chosen was day 10, and the resulting streamfunctions after 12 h and 1 day of integration are shown in Fig. 12. Comparison with Fig. 2 reveals a close similarity between these barotropic solutions and the baroclinic solutions at days 11 and 12. Evidently the essential features of the decay are reproduced by the barotropic vorticity equation, although the time scale of the motion is about half that given by the primitive equations. This is consistent with Fig. 5, which shows some continued baroclinic conversion from eddy available potential energy to eddy kinetic energy and from zonal kinetic energy to zonal available potential energy during the decay stage. Similar results are found for the other wavenumber 6 disturbances.

A disadvantage of the above experiments is that considerable change in the upper-level structure had occurred in the baroclinic integrations by the day chosen to begin the barotropic simulations, the momentum flux already being predominantly poleward for the wavenumber 6 examples. A second set of barotropic integrations was thus performed using the same *initial* flow as that at $\sigma=0.321$ in the baroclinic experiments except that the amplitude of the normal mode perturbation was increased so as to be similar to the largest value reached in the full nonlinear integration. For wavenumber 6 these experiments were characterized not only by an initial decay of wave amplitude as implied by the energetics of the normal mode, but also by rapid changes in phase tilt in the sense observed more gradually during the finite-amplitude growth and decay stages of the baroclinic disturbances.

Some results for the 45° jet are shown in Fig. 13 in which is plotted the initial phase of the wavenumber 6 component of the streamfunction as a function of latitude, and the phase after 12 h of integration for three experiments. Curve A is that obtained from a nonlinear

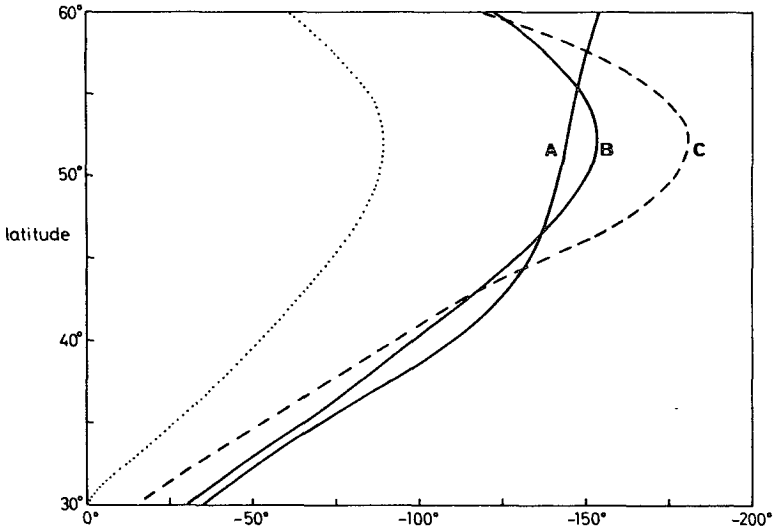

FIG. 13. Variation with latitude of the initial phase of zonal wavenumber 6 (dotted curve), and the phase after 12 h of barotropic integration for three cases specified in the text.

solution of the barotropic vorticity equation with triangular truncation at total wavenumber 42. It indicates an increase of the preexisting phase tilt equatorward of 42° latitude, and a slight decrease between 42° and 52°. In the initial mode the phase tilt is reversed poleward of 52°, but changes in this region are such that this reversal disappears within 12 h of integration to give a momentum flux that is everywhere poleward. The corresponding linear solution, curve B, shows a similar overall movement of the disturbance but no net reduction of the reversed phase tilt.

Further experiments have been performed. For brevity we summarize our results by noting that phase changes at each particular latitude are determined largely by the *local* zonal-mean flow and latitudinal gradient of absolute vorticity. In a barotropic normal mode, advection by the local mean flow and propagation due to the local vorticity gradient produce the same movement at different latitudes as a consequence of a particular meridional structure of the mode which depends on the mean flow at other latitudes. Here the initial structure is not a normal mode for the barotropic equation, and the marked latitudinal variations in phase speed are much as suggested by latitudinal variations in the mean flow and length scale of the initial wave. An essentially similar behavior was recognized synoptically by Namias and Clapp (1944). In the nonlinear integration (curve A) sharpening of the westerly jet enhances the poleward vorticity gradient in middle latitudes, but reduces it to north and south, giving a strong reversal of gradient near 60°. Differences between curves A and B are consistent with the expected resulting change in phase movement. Confirmation that it is the change in mean-flow vorticity gradient that is important for the removal of the reversed phase tilt is provided by the different form of curve C, which was obtained from a nonlinear integration in which changes in this mean gradient were artifically suppressed.

For the wavenumber 9 disturbance to the 45° jet, barotropic integrations successfully reproduced the decay of wave amplitude, but this decay was accompanied by an increase in the strength of the poleward component of the momentum flux relative to the equatorward component, the opposite change to that which occurs gradually over the course of the baroclinic integration. The difference is insignificant, however, since the absolute amplitudes of the poleward components remain of the order of 1–2 $m^2 s^{-2}$ or less.

9. Quasi-barotropic motion in a baroclinic fluid

In the preceding section it was shown that the barotropic vorticity equation can give an accurate simulation of the decay stage at upper levels for wavenumber 6 but on a time scale about half that found in the full baroclinic model. We now show how such a result follows from the quasi-geostrophic system of equations upon introducing two further approximations.

Following for simplicity of presentation the formulation given by Hoskins *et al.* (1978) for an *f*-plane, the vorticity and temperature equations in the quasi-geostrophic system may be written

$$\left[\frac{\partial}{\partial t}+\mathbf{v}\cdot\nabla\right]\xi=f\frac{\partial w}{\partial z}, \tag{9.1}$$

$$\frac{g}{\theta_0}\left[\frac{\partial}{\partial t}+\mathbf{v}\cdot\nabla\right]\theta=-N^2w. \tag{9.2}$$

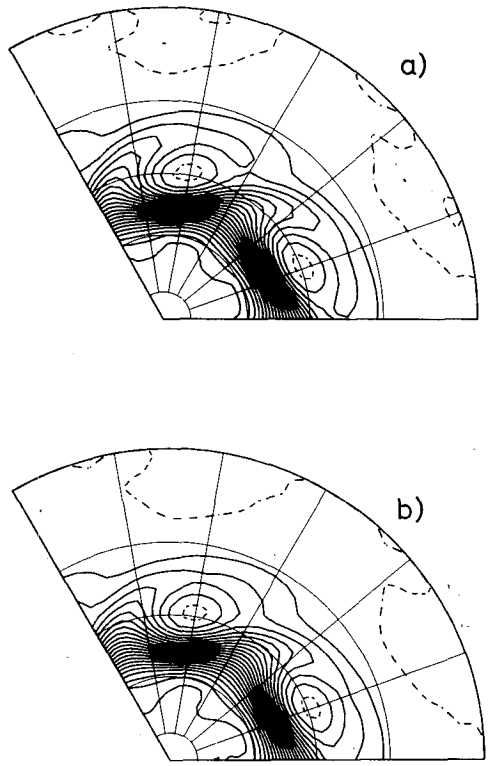

FIG. 14. Quasi-geostrophic simulations of the decay stage. Details are specified in the text.

Here $\mathbf{v}$ is the horizontal geostrophic velocity, ξ the geostrophic vertical component of relative vorticity, and other symbols are as used by Hoskins *et al.* (1978). A diagnostic equation for vertical motion (a form of the usual omega equation) is obtained by eliminating time derivatives from (9.1) and (9.2) using the thermal wind relation, which gives

$$N^2\nabla^2 w + f^2\frac{\partial^2 w}{\partial z^2} = f\frac{\partial}{\partial z}(\mathbf{v}\cdot\nabla\xi) - \frac{g}{\theta_0}\nabla^2(\mathbf{v}\cdot\nabla\theta). \quad (9.3)$$

The forcing of vertical motion is by the vertical derivative of vorticity advection, the first term on the right-hand side of (9.3), and by the horizontal Laplacian of thermal advection.

Hoskins *et al.* (1978) have drawn attention to possible drawbacks in using the forcing terms as in (9.3) and have suggested use of a different, though equivalent, expression. Two drawbacks noted were the tendency for the two terms to cancel in a growing baroclinic wave, and the lack of invariance of these terms under the addition of a uniform velocity. However, for the present purpose of describing the rapid decay of a finite-amplitude baroclinic wave, it is convenient to retain the form given above since, as will be shown, in a particular coordinate system one of the forcing terms is negligible.

The coordinate system is one fixed in the surface of the earth. Evaluation of the two terms for the wavenumber 6 disturbance to the 45° jet shows that in the growing mode thermal and vorticity advection are of similar importance, but the former is larger at lower than at upper tropospheric levels. Subsequently, as low-level temperature gradients are weakened in the region of maximum eddy activity, the thermal forcing becomes significantly weaker.

The resulting negligible role of thermal advection in forcing vertical motion during the decay stage is illustrated by integrations performed using a five-layer version of the quasi-geostrophic model described by Simmons and Hoskins (1976). Initial fields were taken from day 10 of a five-layer primitive-equation integration, details of which are given in the following section. The streamfunction at $\sigma=0.3$ after one day's integration is shown in Fig. 14a for the complete quasi-geostrophic model, while Fig. 14b shows the corresponding field for an integration in which the thermal forcing of vertical motion [given for the spherical model by the second line of Eq. (B5) of Simmons and Hoskins (1976)] was suppressed. The similarity of the two plots demonstrates the unimportance of the thermal forcing at this stage of the life cycle. Similar agreement is found a day later, by which time the wave is of small amplitude, very much as shown in Fig. 2 for day 12 of the higher resolution primitive-equation integration.

To reach a form of the barotropic vorticity equation, as well as neglecting thermal advection, a more crude approximation is necessary. We introduce a height scale H and length scale L and assume approximate sinusoidal behavior of w in the vertical and horizontal. Eq. (9.3) then implies

$$f\frac{\partial w}{\partial z} = \left[\frac{1}{1+N^2H^2/f^2L^2}\right]\mathbf{v}\cdot\nabla\xi$$

and substitution in (9.1) yields

$$\left[1+\frac{f^2L^2}{N^2H^2}\right]\frac{\partial\xi}{\partial t} = -\mathbf{v}\cdot\nabla\xi. \quad (9.4)$$

This is of the same form as the barotropic vorticity equation, but with time scaled by a factor $(1+f^2L^2/N^2H^2)^{-1}$, typically about a half for a baroclinic wave. This argument is unlikely to be reliable in regions of small vorticity advection, but results presented in the preceding section suggest it gives an accurate representation for the upper troposphere where vorticity advection is close to its maximum value. At such levels barotropic processes become dominant as low-level thermal advection decreases with the occlusion of the disturbance, but the response of the vorticity field is about half that which would occur in a barotropic fluid because of adjustment of the temperature field to maintain thermal wind balance.

It should be stressed that the general notion of baroclinic growth followed by a quasi-barotropic

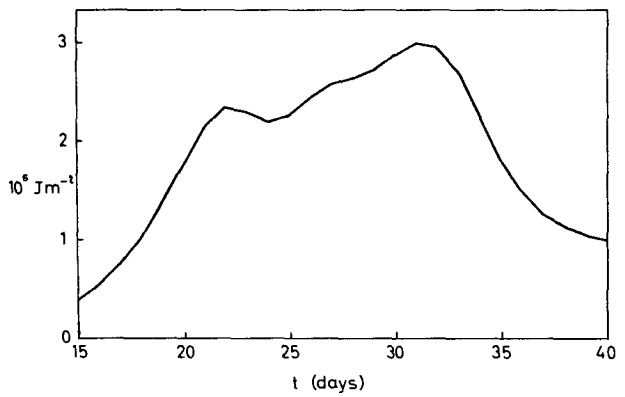

FIG. 15. Variation with time of the net eddy energy for an initial wavenumber 3 perturbation of the broad 30° jet.

behavior is by no means new, having been identified in early barotropic forecasts by Charney *et al.* (1950) and discussed extensively in an oceanographic context by Rhines (1977). The analysis given in this section is in part similar to the earlier derivation of an "equivalent-barotropic" model (e.g., Thompson 1961), and if $-L^2\xi$ is replaced by a streamfunction ψ in (9.4) we obtain

$$\frac{\partial}{\partial t}\left[\xi-\frac{f^2}{N^2H^2}\psi\right]+\mathbf{v}\cdot\nabla\xi=0,$$

an equation identical in form to one derived by Wiin-Nielsen (1959) to improve barotropic forecasts of long-wave behavior. Barotropic models have been used traditionally to forecast the 500 mb flow, but the present results show that such a model may on occasions work well at an upper-tropospheric level.

10. Some further primitive-equation experiments

a. Other wavenumbers

Two additional integrations, with initial disturbances in wavenumbers 3 and 12, respectively, have been performed for the broader 30° jet. The linear growth rate of wavenumber 3 is less than half that of 6 and 9, and results in this case are of particular interest in that after the initial growth of wavenumber 3 they describe the development of large-amplitude disturbances of shorter zonal scale and the subsequent growth of a longer wave component.

The variation of total eddy energy for the wavenumber 3 experiment is illustrated in Fig. 15 which again shows periods of growth and decay. The corresponding surface pressure fields reveal first the growth of wavenumber 3 and then the development of two low-pressure centers of a scale similar to that of zonal wavenumber 6 disturbances. One of these reaches a maximum amplitude at day 26, and subsequently merges with the other to form a single larger scale low at day 30. The latter develops slightly and then decays. The spectral decomposition of the vorticity indicates a maximum in zonal wavenumber 6 at about day 26, with a generation of wavenumber 3 and to a lesser extent zonal components up to day 32. The amplitudes of dominant wavenumber 3 components decrease beyond this time, along with an overall transfer of eddy energy to the zonal-mean state. The slight drop in eddy energy between days 22 and 24 indicated in Fig. 15 may result from a difference in phase between the wavenumber 3 component growing as a result of the initial normal-mode perturbation and a component nonlinearly forced as the shorter scale disturbances mature, since several of the principal wavenumber 3 components of vorticity are found to decrease to small amplitude and rapidly change phase at about this time.

Meridional cross sections of the poleward eddy fluxes of heat and momentum averaged from day 18 to day 38 are shown in Fig. 16. Comparison with the corresponding results for wavenumber 6 initial conditions (Figs. 7b and 8b) reveals a very close agreement, particularly for the momentum flux. The heat flux extends further poleward, a consequence of a significant contribution from transfer by the longer wavelength disturbance generated later in the integration. This transfer is a maximum at day 30, and is located nearer the pole than is the transfer by the earlier disturbances with the scale of wavenumber 6. The ratio of the averaged

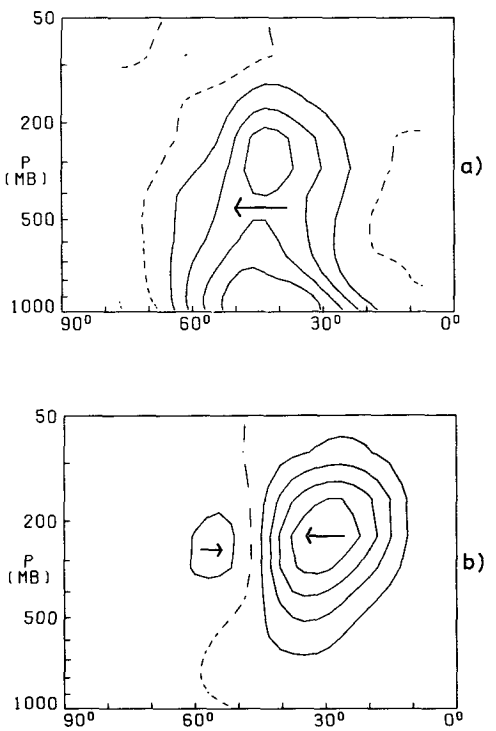

FIG. 16. Meridional cross sections of (a) the time-averaged horizontal eddy heat flux and (b) the corresponding momentum flux for the wavenumber 3 experiment.

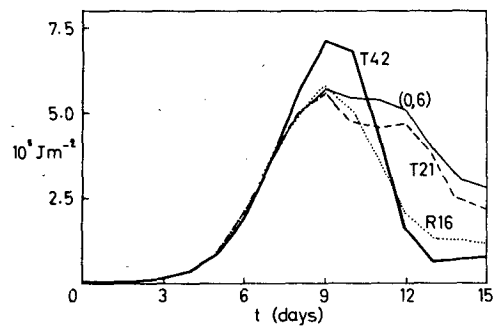

FIG. 17. Variation with time of the net eddy energy for the wavenumber 6 disturbance to the 45° jet integrated using triangular truncation at total wavenumber 42 (T42), triangular truncation at wavenumber 21 (T21), rhomboidal truncation at zonal wavenumber 16 (R16) and a severe zonal truncation [(0, 6)].

heat and momentum fluxes is close to that found for wavenumber 6 initial conditions, and the maximum eddy kinetic energy density is relatively larger by about 50%, in closer agreement with observation. The overall similarity of eddy fluxes provides some evidence that our results are not particularly sensitive to the specification of rather special normal-mode initial conditions.

Results from the wavenumber 12 integration are of less interest, being much as found for wavenumber 9 apart from weaker amplitudes and a vertical structure more concentrated at the surface. Although faster growing short-wavelength disturbances can result from the inclusion of moisture and from different choices of flow profile (Gall, 1976c; Simmons and Hoskins, 1977b), both observed upper tropospheric flow patterns and results from Gall's moist model indicate that the upper level amplitudes of such disturbances are small compared with those of the lower wavenumber disturbances examined in detail in this paper.

b. Numerical resolution

A number of integrations have been performed using different spatial resolutions for the case of the 45° jet with wavenumber 6 initial conditions. These have been performed partly to confirm the absence of any significant truncation error in the results discussed in preceding sections, and partly to examine the ability of lower resolution models to simulate accurately the complete life cycle of the disturbance.

We consider first variations in horizontal resolution. An integration using triangular truncation at total wavenumber 63 has been performed using as initial conditions, for economy, the results from the wavenumber 42 integration at day 5. To avoid an expensive reduction in time step the diffusion coefficient κ was halved, and comparison made with a wavenumber 42 integration that used a similar diffusion. Differences were small, typically of the order of a few percent for maximum eddy energies, averaged fluxes and zonal-mean changes, and about a fifth the size of the differences that resulted from changing the diffusion coefficient. The latter are discussed further in the following subsection.

Three lower resolution integrations have also been performed. These comprised runs with triangular truncation at total wavenumber 21 and rhomboidal truncation at zonal wavenumber 16, together with a zonally truncated version retaining only zonal-mean and wavenumber 6 components, meridional resolution being as in triangular truncation at wavenumber 42. The resulting variation in eddy energy shown in Fig. 17 indicates close agreement up to day 7. Maximum energies reached at day 9 are 20% lower in all three lower resolution integrations, agreement being apparently fortuitous as there are larger but cancelling differences in energy conversions at day 8.

Results beyond day 9 show more substantial differences. The rhomboidal integration captures the relatively rapid decay in wave amplitude found in higher resolution results, but the other two show little initial decay and generally less loss of eddy energy, with averaged poleward momentum fluxes that are only about half that obtained using higher resolutions. The rhomboidal resolution used here represents the hemispheric meridional structure of zonal wavenumber 12 by eight nonzero modes, just three more than in the lower resolution triangular truncation, but these additional modes appear to give rise to a much more accurate representation of the decay. Care should be taken in interpreting this as evidence favoring rhomboidal truncation for general use, since for relatively low resolution the appropriate choice of truncation appears to be quite dependent on the particular nature of the problem under investigation (Simmons and Hoskins, 1975).

Vertical resolution has been examined briefly by performing two additional integrations. In the first a 16-layer model was used, the layer spacing being as described by Simmons and Hoskins (1977a). This gave a lower resolution near the surface, and an improved stratospheric resolution. Insignificant tropospheric changes were found, and reference has already been made to some of the quantitative differences found in the lower stratosphere.

In the second experiment five equally spaced layers were used. The resulting variation with time of the net eddy energy is compared with that from the standard 14-layer model in Fig. 18. Agreement is seen to be close. Strict comparisons of eddy fluxes and zonal-mean changes are made difficult by the different locations of model levels, but maximum values obtained from the five layer model are in most cases no more than 10% weaker than values interpolated to corresponding levels from 14-layer results. The five-layer model thus appears adequate to simulate the main tropo-

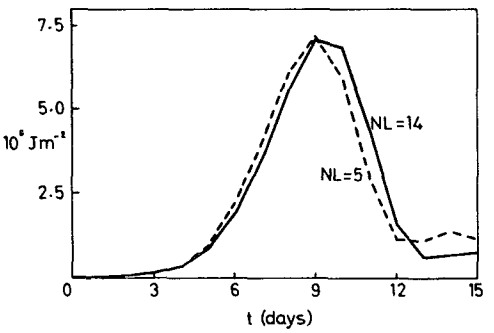

FIG. 18. As Fig. 17, but for two different vertical resolutions, denoted by NL (the number of layers). The horizontal resolution is T42.

spheric features of the wavenumber 6 disturbance to the 45° jet. Experience with linear calculations (Simmons and Hoskins, 1976) suggests it would be unreliable for most shorter scales.

c. *Internal diffusion*

As noted in Section 2, the inclusion of some form of internal dissipation is necessary in experiments such as these, but the form and magnitude chosen vary widely in different numerical models. To obtain some indication of the sensitivity of our results in this respect several experiments have been performed with different choices. For the wavenumber 6 disturbance to the 45° jet these comprised halving the coefficient κ everywhere, reducing it above $\sigma=0.5$ to a quarter of its standard value, and doubling it everywhere as applied to vorticity and divergence but halving it as applied to temperature. Resulting changes were small, amounting to at most 10% for the averaged eddy heat and momentum fluxes, and up to 20% for the more subtle net change to the upper level zonal-mean flow. Such differences are insignificant in the present context in view of marked quantitative differences from flow to flow and qualitative differences between wavenumbers 6 and 9.

The smaller zonal and meridional length scales of wavenumber 9 disturbances render them more sensitive to internal dissipation, but here too we find relatively small differences. For the 45° jet, halving the diffusion coefficient resulted in an increase of some 20% in eddy energies, net heat and momentum fluxes, and zonal-mean changes.

Recent analytical studies of the interaction between waves and the zonal-mean state (Andrews and McIntyre, 1976; Boyd, 1976) have generalized earlier work and reemphasized the crucial importance of transience and dissipation in bringing about zonal-mean changes. With this in mind it should be noted that our finding that net changes are not particularly sensitive to the formulation of the internal dissipation does not imply that dissipation itself is unimportant. We have already noted that over the life cycle of the wavenumber 6 disturbance to the 45° jet the net dissipation accounts for about as much of the loss of zonal available potential energy as does the gain in zonal kinetic energy. In the corresponding experiments with different forms of diffusion, compensating changes in the amplitudes of smaller scales result in net dissipations which differ by less than 25%. The lack of sensitivity to the precise formulation suggests the possibility that the dissipation is mainly determined by the large-scale motion. This is consistent with theoretical work (e.g., Hoskins and Bretherton, 1972) that envisages frontogenesis as being a direct result of the large-scale flow in a growing baroclinic eddy.

d. *Other physical processes*

An obviously unrealistic feature of our results is the intensity of the surface flow that develops over the course of each integration, this reaching a westerly maximum of over 30 m s^{-1} for the wavenumber 6 disturbance to the 45° jet. This latter case has thus been recomputed incorporating a simple representation of surface friction. The precise form is specified in an Appendix.

Results differ little in most respects. The presence of surface friction slows the development by about a day, but averaging fluxes from day 5 to day 15 we find very similar overall patterns, as may be seen by comparing Fig. 19 with Figs. 7a and 8a. The maximum upper

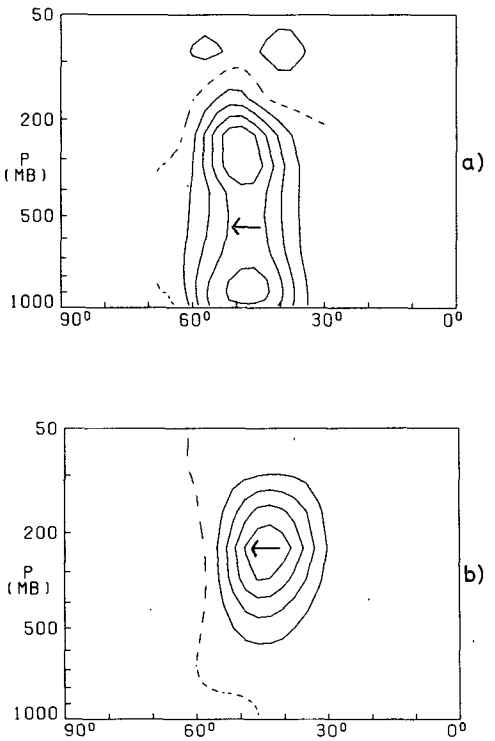

FIG. 19. Meridional cross sections of (a) the time-averaged horizontal eddy heat flux and (b) the corresponding momentum flux for the wavenumber 6 disturbance to the 45° jet with surface friction included.

level momentum fluxes are some 10% weaker and heat fluxes differ by 5%. The induced surface westerly maximum is indeed significantly reduced to little over 10 m s^{-1}, and there is a substantial change in the mean meridional circulation at low levels. Consistent with this there is a substantially smaller net reduction of the mid-latitude temperature gradient in the lower troposphere, as shown in Table 2, and the upper level westerly jet is only some 4 m s^{-1} weaker at day 15.

In addition, wavenumber 6 integrations similar to those discussed in this paper are being used to examine the parameterization and role of various other physical processes. Initial experiments have used a five-layer vertical resolution, and they include examples in which the mid-latitude temperature gradient is restored by diabatic heat sources during the course of the integration. Preliminary results indicate quantitative modifications, but all cases exhibit an initial baroclinic growth followed by barotropic decay, giving at least a first cycle similar to that described here.

11. Summary and concluding remarks

It is evident from these integrations that nonlinearity can significantly modify several results of linear stability theory. Finite-amplitude disturbances exhibit more baroclinic growth at upper than lower levels, and a subsequent quasi-barotropic behavior. Related changes in structure are of particular significance in that the largest eddy fluxes occur close to the time of maximum eddy energy, when deviations from linear theory are marked. One result is that net eddy fluxes of both heat and momentum have upper level amplitudes substantially larger relative to surface values than given by linear stability analyses, and agreement with observation is improved.

Barotropic processes become important as the disturbance occludes, although the three-dimensional nature of the motion is such that the response of the vorticity field is about half that which would occur in a barotropic fluid. Eddy momentum fluxes become stronger relative to heat fluxes, and predominantly poleward for the longer wavelength disturbances which dominate at upper levels. These changes are also such as to bring results into closer agreement with observation. In the present examples we find a barotropic decay of wave energy at a rate similar to that of baroclinic growth.

The rapid growth, change in structure and decay discussed here should not be confused with the vacillation found for weakly unstable disturbances (e.g., Pedlosky, 1972). The development of larger amplitudes at upper levels has been noted previously by Gall (1976b), although the effect is more pronounced in several of the present examples. Simons (1972) commented on an increase in the relative strength of the barotropic energy conversion as a baroclinic wave grew into the nonlinear regime, but further accurate integration was prevented by insufficient numerical resolution. Our own results using different resolutions suggest that accurate simulation of the decay requires a finer resolution than does that of the growth, and may account for the absence of any discussion of a decay stage in Gall's paper.

Over the full life cycle, reduction of the mid-latitude temperature gradient is principally confined to lower levels. Sharper gradients are formed in shallow regions to south and north, a consequence of the limited meridional scale of disturbances, but no significant secondary development occurs in these regions in the present experiments. Any such development that might take place in other examples would be likely to be of small vertical scale, and thus unlikely to alter the upper level structure found here.

In the upper troposphere reduction of the mid-latitude temperature gradient as the wave grows is compensated by a subsequent increase as the upper level jet strengthens, and little net change results. Lower stratospheric temperature gradients are increased above the jet maximum, thus remaining in approximate thermal-wind balance. The change in surface zonal flow is of the pattern found in normal-mode solutions, with a region of westerlies bounded by regions of easterly flow. The maximum strength of the upper level zonal-mean flow is almost constant throughout the growth period, and the production of a stronger, narrower jet takes place over a limited period as the wave decays.

Several of our results have implications for the accurate parameterization of eddy fluxes for use in climate models which do not include an explicit representation of unstable baroclinic disturbances. The marked changes in wave structure over the course of these nonlinear integrations indicate that use of linear theory to determine the spatial structure of eddy fluxes is unlikely to yield realistic results. The qualitative similarity in structure for different zonal flows is encouraging, momentum fluxes showing less variability than in linear solutions, but large variations in magnitude have been found. In these examples growth ceases shortly after the surface temperature gradient is first destroyed at some latitude. Linear theory provides a guide to the time at which this occurs, but does not give a precise indication of the maximum amplitude reached.

The large differences between wavenumber 6 and wavenumber 9 may also pose difficulty for an eddy-flux parameterization. Differences between these wavenumbers in linear calculations have been found to be enhanced in the nonlinear regime, and it thus appears necessary in a parameterization to specify the spectral distribution of eddy fluxes. Knowledge of the linear growth-rate spectrum may be of help in this respect, but it is not clear that this is sufficient.

The markedly different vertical structure of wavenumbers 6 and 9 is consistent with the classical synoptic distinction between "long waves" (with zonal wavenumbers 3–7) which typically dominate the upper level flow and shorter, shallower "cyclone waves," several of which may develop in succession superimposed on a relatively stationary long-wave pattern (Palmén and Newton, 1969). Although the shorter waves are responsible for much of the day-to-day variability of surface weather in middle latitudes, their individual influence on the upper flow is weak, much as found here for wavenumber 9. Studies of the longer waves (e.g., Cressman, 1948) have noted their tendency to remain almost stationary for several days, but emphasis has also often been placed on their growth, distortion or decay since a change in long-wave pattern may bring about a basic change in weather type, and thus may be of importance for extended range forecasting.

Such synoptic considerations lead us to stress, in conclusion, that we have examined some nonlinear aspects of baroclinic waves in what is still, in comparison with the atmosphere, a very simple situation. In particular, baroclinic growth and barotropic decay of a wave take place with identical disturbances and jets both upstream and downstream. Examination of either sequences of 300 mb charts or past synoptic studies (e.g., Newton *et al.*, 1951) does indeed reveal events resembling those illustrated in Fig. 2, but a variety of other behavior may also be observed. Thus the barotropic decay discussed here, and associated effects on eddy fluxes and the zonal-mean state, should be regarded not as general properties of mature atmospheric systems, but rather as properties of one particular type of atmospheric behavior. It is our intention to examine other situations in future studies.

Acknowledgments. We are grateful to D. G. Andrews and R. P. Pearce for helpful comments.

APPENDIX

The Surface Friction Formulation

As a very simple surface friction appropriate to a model with several layers close to the ground we include no frictional term above $\sigma = 0.75$, while at lower levels we add a term

$$-F(4\sigma-3)|\mathbf{v}_s|\mathbf{v}_s$$

to the expression for the rate of change of the horizontal velocity vector $\mathbf{v}$. Here $F=8\times10^{-7}$ m^{-1} and $\mathbf{v}_s$ is the velocity at the lowest model level, $\sigma=0.985$. This formulation is approximately equivalent to a stress which decreases from a surface value

$$-\rho_s C_D|\mathbf{v}_s|\mathbf{v}_s, \quad C_D=0.001,$$

to zero at a height of 2.5 km, this decrease occurring with a quadratic dependence on height.

REFERENCES

Andrews, D. G., and M. E. McIntyre, 1976: Planetary waves in horizontal and vertical shear: The generalized Eliassen-Palm relation and the mean zonal acceleration. *J. Atmos. Sci.*, **33**, 2031–2048.

Blackmon, M. L., J. M. Wallace, N.-C. Lau and S. L. Mullen, 1977: An observational study of the Northern Hemisphere wintertime circulation. *J. Atmos. Sci.*, **34**, 1040–1053.

Boyd, J. P., 1976: The noninteraction of waves with the zonally-averaged flow on a spherical earth and the interrelationships of eddy fluxes of energy, heat and momentum. *J. Atmos. Sci.*, **33**, 2285–2291.

Charney, J. G., 1947: The dynamics of long waves in a baroclinic westerly current. *J. Meteor.*, **4**, 135–162.

——, R. Fjörtoft and J. von Neumann, 1950: Numerical integration of the barotropic vorticity equation. *Tellus*, **2**, 237–254.

Cressman, G. P., 1948: On the forecasting of long waves in the upper westerlies. *J. Meteor.*, **5**, 44–57.

Eady, E. T., 1949: Long waves and cyclone waves. *Tellus*, **1**, 33–52.

Gall, R., 1976a: A comparison of linear baroclinic instability theory with the eddy statistics of a general circulation model. *J. Atmos. Sci.*, **33**, 349–373.

——, 1976b: Structural changes of growing baroclinic waves. *J. Atmos. Sci.*, **33**, 374–390.

——, 1976c: The effects of released latent heat in growing baroclinic waves. *J. Atmos. Sci.*, **33**, 1686–1701.

Green, J. S. A., 1970: Transfer properties of large-scale eddies and the general circulation of the atmosphere. *Quart. J. Roy. Meteor. Soc.*, **96**, 157–184.

Hoskins, B. J., and F. P. Bretherton, 1972: Atmospheric frontogenesis models: Mathematical formulation and solution. *J. Atmos. Sci.*, **29**, 11–37.

——, and A. J. Simmons, 1975: A multi-layer spectral model and the semi-implicit method. *Quart. J. Roy. Meteor. Soc.*, **101**, 637–655.

——, I. Draghici and H. C. Davies, 1978: A new look at the ω-equation. *Quart. J. Roy. Meteor. Soc.*, **104**, 31–38.

Kuo, H.-L., 1953: On the production of mean zonal currents in the atmosphere by large disturbances. *Tellus*, **5**, 475–493.

Lorenz, E. N., 1955: Available potential energy and the maintenance of the general circulation. *Tellus*, **7**, 157–167.

Namias, J., and P. F. Clapp, 1944: Studies of the motion and development of long waves in the westerlies. *J. Meteor.*, **1**, 57–77.

Newell, R. E., J. W. Kidson, D. G. Vincent and G. J. Boer, 1972: *The General Circulation of the Tropical Atmosphere, and Interactions with Extratropical Latitudes*, Vol. 1. The MIT Press, 258 pp.

——, ——, —— and ——, 1974: *The General Circulation of the Tropical Atmosphere, and Interactions with Extratropical Latitudes*, Vol. 2. The MIT Press, 371 pp.

Newton, C. W., N. A. Phillips, J. E. Carson and D. L. Bradbury, 1951: Structure of shear lines near the tropopause in summer. *Tellus*, **3**, 154–171.

Oort, A. H., and E. R. Rasmusson, 1971: Atmospheric circulation statistics. NOAA Prof. Pap. 5. [U. S. Govt. Printing Office, Stock No. 0317-0045, c 55.25:5.]

Palmén, E., and C. W. Newton, 1969: *Atmospheric Circulation Systems*. Academic Press, 603 pp.

Pedlosky, J., 1972: Limit cycles and unstable baroclinic waves. *J. Atmos. Sci.*, **29**, 53–63.

Platzman, G. W., 1952: The increase or decrease of mean-flow energy in large-scale horizontal flow in the atmosphere. *J. Meteor.*, **9**, 347–358.

Rhines, P. B., 1977: The dynamics of unsteady currents. *The Sea*, Vol. 6, Wiley (see pp. 189–318).

Robert, A., 1966: The integration of a low order spectral form of the primitive meteorological equations. *J. Meteor. Soc. Japan*, **44**, 237–245.

Schneider, S. H., and R. E. Dickinson, 1974: Climate modeling. *Rev. Geophys. Space Phys.*, **12**, 447–493.

Simmons, A. J., and B. J. Hoskins, 1975: A comparison of spectral and finite-difference simulations of a growing baroclinic wave. *Quart. J. Roy. Meteor. Soc.*, **101**, 551–565.

——, and ——, 1976: Baroclinic instability on the sphere: Normal modes of the primitive and quasi-geostrophic equations. *J. Atmos. Sci.*, **33**, 1454–1477.

——, and ——, 1977a: Baroclinic instability on the sphere: Solutions with a more realistic tropopause. *J. Atmos. Sci.*, **34**, 581–588.

——, and ——, 1977b: A note on the wavelength of maximum growth rate for baroclinic instability. *J. Atmos. Sci.*, **34**, 1477–1478.

Simons, T. J., 1972: The nonlinear dynamics of cyclone waves. *J. Atmos. Sci.*, **29**, 38–52.

Thompson, P. D., 1961: *Numerical Weather Analysis and Prediction.* Macmillan, 170 pp.

White, A. A., 1977: The surface flow in a statistical climate model—a test of a parameterization of large-scale momentum fluxes. *Quart. J. Roy. Meteor. Soc.*, **103**, 93–119.

Wiin-Nielsen, A., 1959: On barotropic and baroclinic models, with special emphasis on ultra-long waves. *Mon. Wea. Rev.*, **87**, 171–183.